POLITECNICO
MILANO 1863

RE.PUBLIC@POLIMI
Research Publications at Politecnico di Milano

Post-Print

This is the accepted version of:

P. Zhou, H. Ren, W. Fan, P. Masarati
Efficient explicit integration for dynamics of inextensible ANCF beams with large deformations
Nonlinear Dynamics, Vol. 113, p. 26033-26048, 2025 (published online 07/06/2025)
doi:10.1007/s11071-025-11433-4

This is a post-peer-review, pre-copyedit version of an article published in Nonlinear Dynamics. The final authenticated version is available online at: https://doi.org/10.1007/s11071-025-11433-4

Access to the published version may require subscription.

When citing this work, cite the original published paper.

Permanent link to this version
http://hdl.handle.net/11311/1292165

Efficient explicit integration for dynamics of inextensible ANCF beams with large deformations[1]

Ping Zhou[†], Hui Ren[†], Wei Fan[†,*], Pierangelo Masarati[‡,*]

[†] School of Astronautics, Harbin Institute of Technology, Harbin, P.R. China

zhouping@hit.edu.cn, renhui@hit.edu.cn, fanwei@hit.edu.cn

[‡]Department of Aerospace Science and Technology, Politecnico di Milano, via La Masa 34, Milan, Italy

pierangelo.masarati@polimi.it

[*]Corresponding author

Abstract

Explicit integration in flexible multibody dynamics is highly attractive for real-time simulation but poses significant efficiency challenges. The bending and axial straining dynamics of slender structural components, such as beams and cables, operate on different time scales. As a result, axial straining—usually the higher-frequency one, though often of minor interest—imposes strict time step limitations for algorithmic stability in explicit integration schemes. This work achieves efficient explicit integration for inextensible flexible beams undergoing large deformations. The key is to develop a dynamic model optimized for explicit integrators by reducing the stiffness of the problem. To this end, an absolute nodal coordinate formulation for inextensible beams is proposed, where the elastic potential energy is derived from the direct multiplication of the first and second derivatives of the position vector with respect to the arc-length coordinate. This formulation results in equations of motion with moderate stiffness, making it well-suited for explicit schemes. Inextensibility is rigorously enforced through algebraic constraints on slope vector lengths, applied either at discrete points or via a fixed-length constraint on the entire span of the beam. A constraint stabilization technique is employed to transform the resulting system of differential-algebraic equations into a set of ordinary differential equations, ensuring numerical stability. The main advantage of this method is its ability to accommodate large time steps, significantly improving computational efficiency. This capability makes explicit simulation schemes more practical and contributes to enabling real-time simulation of mechanical systems with flexible beams or cables.

keywords: explicit integration, inextensible beams, absolute nodal coordinate formulation, dynamic modeling, algebraic constraints

1 Introduction

Efficient explicit integration is essential in many applications requiring real-time simulations, such as industrial mobile machinery [1], model predictive control [2], real-time hybrid testings [3], and automatic vehicle driving [4, 5]. Explicit real-time simulations offer advantages over implicit ones, including high parallelism, low complexity, and predictable computational costs, making them highly desirable in engineering applications.

Explicit integration schemes are effective in non-stiff problems with good accuracy in multi-rigid-body systems [6, 7, 8, 9] because no Newton iterations are required in the simulation. A critical drawback is their relatively small stability regions; therefore, compared to those of implicit schemes, the usable time step sizes can be tremendously restricted when stiff problems are integrated. For very flexible bodies with a low elastic modulus, implicit and explicit methods show no significant differences in accuracy and computational effort [10]. However, as stiffness increases, the equations become stiffer, making explicit methods less effective. Generally, conventional explicit schemes are unable to tackle mechanical systems with flexible bodies because the associated high frequencies can make the dynamic equations excessively stiff.

Two strategies can be taken to solve the dynamics of flexible systems using explicit methods. The first strategy is to develop methods with larger stability zones. For example, the stabilized Runge-Kutta integrators with large stability regions can tackle mildly stiff problems, because their stability regions can be arbitrarily extended along the negative axis by adjusting the number of stages [6, 11]. The predictor-corrector explicit version of the generalized-α method was proposed to provide an optimal combination of low-frequency and high-frequency dissipation [12, 13], which can handle structural problems well.

The other strategy aims to reduce the stiffness of flexible systems by developing elegant dynamic models that make their explicit simulation effective. For example, in the simulation of Cosserat rods, strong damping can be imposed on the stiff degrees of freedom associated with extension and shearing [14]. Recursive formulæ for beams with reduced stiffness have also been developed, making them suitable for explicit schemes [15, 16]. In addition, the model reduction technique of the global modal parameterization has been utilized to reduce both the stiffness and the number of degrees of freedom of the beam model, making an efficient explicit real-time simulation possible [17]. Despite extensive research, few advancements have been made in the explicit simulation of flexible beams with large deformations using the absolute nodal coordinate formulation (ANCF), which is widely applied in flexible multibody systems.

The ANCF describes the dynamics of flexible bodies undergoing large displacements, rotations, and deformations using absolute position and gradient coordinates [18, 19]. The ANCF elements can be divided into two categories: fully parameterized and gradient-deficient elements. The fully parameterized beam element allows for a general description of axial, shear, bending, torsional, and cross-sectional deformations using all three nodal gradient vector components [20, 21]. However, the high number of generalized coordinates introduces shear and Poisson locking issues that must be mitigated [22]. The gradient-deficient elements use only some of the gradient components by adopting a rigid cross-section or Euler-Bernoulli's assumption. As a result, the number of generalized coordinates decreases and the formulation is much simpler. A gradient-deficient ANCF beam element that employs only the axial gradient vector was proposed to describe beam bending and axial deformations [23]. This ANCF beam model accurately captures bending and extension and has been extended for efficient modeling of slender cables in power transmission line problems [24]. It also led to the development of the variational spacetime ANCF formulation [25, 26]. Despite their popularity in engineering applications where large deformations stem primarily from bending, little research has focused on the effective explicit simulation of inextensible beam models [27]. Unlike strain-based formulations [28], where axial strain can be artificially introduced or removed, ANCF inherently accounts for it by using axial gradients as generalized coordinates. Up to now, the explicit simulation and effective dynamical modeling of inextensible ANCF beams are still an open problem and in high demand.

This work presents efficient explicit integration of the inextensible ANCF beams with large deformation. The derivation of the present formulation is more straightforward and greatly simplified compared to conventional elements. The present formulation resembles the gradient-deficient ANCF model since only the position vector and its slopes are employed. It differs from existing research because, to improve the computational efficiency, the high frequencies of the beam are reduced by deducing the elastic potential energy from a direct multiplication of the first and second derivatives of the position vector with respect to the arc-length coordinate. The inextensibility in the axial direction is guaranteed by introducing fixed length constraints either at the nodal level or globally. To solve constrained systems, a constraint stabilization technique is adopted such that the resulting algebraic differential equations (DAEs) can be transformed into a set of ordinary differential equations (ODEs) with a stabilization parameter. A time-step size selection strategy for explicit schemes is also provided. The novelties of the proposed approach are:

- Curvature is measured by multiplying the magnitudes of the first and second derivatives of the position vector with respect to the arc-length coordinate, effectively capturing the elastic potential energy of an inextensible beam;
- A good accuracy of large lateral deformations is ensured by adding algebraic constraints at the element nodes and fixed-length constraints;
- High frequency components in flexible beams are reduced by omitting axial deformation contributions to the elastic potential energy.
- Larger step sizes can be used with explicit integration schemes based on the present inextensible beam formulation compared to those required by conventional ANCF formulations before algorithmic stability limitations are reached.

The newly developed ANCF formulation enables efficient explicit simulation of constrained inextensible beams, wires, and cables. Furthermore, this method is well-suited for parallel computing, enabling real-time simulations of wire and cable systems.

The structure of this work is as follows: the equations of motion of an inextensible beam ANCF model are derived in Section 2. Section 3 describes the constraint stabilization technique for converting the DAE system into ODEs and outlines the step-size selection strategy for explicit time integration. Section 4 illustrates the capabilities of the explicit integration algorithm through numerical examples. Section 5 summarizes the findings, highlights the formulation's potential, and outlines future research directions.

2 ANCF for Inextensible Beams

This section begins with the derivation of the kinetic energy, elastic potential energy, and virtual work done by external forces. Then, the spatial discretization is performed to obtain the discrete energies and work. To guarantee no axial deformation, nodal constraints of the axial strain at each element node and the fixed length constraints are introduced into the dynamic model. Lastly, by using Lagrange equations with constraints, equations of motion that are DAEs can be derived.

2.1 Kinematics

A flexible beam is considered under the following assumptions:

- The beam is very slender; therefore, the Euler-Bernoulli assumption is adopted and the contribution of the moment of inertia of the beam's cross-section to the kinetic energy is neglected.
- The beam is homogeneous and has a circular cross-section, which is specifically intended for wires and cables. Stretch and bending deformations are decoupled from torsion. Since the latter can be analyzed separately, it is not considered herein for simplicity.
- The strains are assumed to be small so that a linear elastic constitutive law can be used; however, the beam's displacements and deformations are not necessarily small.
- The beam can be considered inextensible along the centroid line.

The arc-length coordinate along the centroid line of the undeformed beam is x; t indicates the time. Let $\boldsymbol{r}(x,t)$ be the position vector of the centroid line of the deformed beam. The kinetic energy of the beam is

$$T = \frac{1}{2}\int_0^L \rho_A \dot{\boldsymbol{r}}^T \dot{\boldsymbol{r}} \mathrm{d}x \tag{1}$$

where the overdot denotes differentiation with respect to time, namely $\dot{\boldsymbol{r}} = \mathrm{d}\boldsymbol{r}/\mathrm{d}t$, L is the length of the undeformed beam, $A = \pi d^2/4$, and ρ_A is its linear density, where d is the diameter of the section.

According to the Euler-Bernoulli assumption, the shear strain is neglected, i.e., $\varepsilon_{12} = \varepsilon_{13} \approx 0$, where direction 1 is along the centroid line, normal to the beam section, whereas the mutually orthogonal directions 2 and 3 lie in the section. The axial strain of the centroid line is

$$\varepsilon = \varepsilon_{11} = \frac{1}{2}\left(\boldsymbol{r}_x^T \boldsymbol{r}_x - \mathring{\boldsymbol{r}}_x^T \mathring{\boldsymbol{r}}_x\right) \tag{2}$$

where $(\cdot)_x$ represents the derivative with respect to x and $\mathring{(\cdot)}$ denotes the corresponding variable in the undeformed configuration. For an inextensible beam, the axial strain should satisfy

$$\varepsilon = 0 \tag{3}$$

Instead of using the material measure of curvature of the beam in the ANCF [29] or the geometrical curvature of a curve calculated by differential geometry [30], the following measure of the cable straining is firstly introduced here

$$\kappa^2 = \|\boldsymbol{r}_x\|^2 \|\boldsymbol{r}_{xx}\|^2 \tag{4}$$

(dimensionally the inverse of a length squared), where $(\cdot)_{xx}$ represents the second derivative with respect to x, and $\|\boldsymbol{r}_x\| = \sqrt{\boldsymbol{r}_x^T \boldsymbol{r}_x}$ and $\|\boldsymbol{r}_{xx}\| = \sqrt{\boldsymbol{r}_{xx}^T \boldsymbol{r}_{xx}}$. Since a circular cross-section was assumed, the bending stiffness is the same in all directions. The elastic potential energy of the beam is

$$U = \frac{1}{2}\int_0^L EI\kappa^2 \mathrm{d}x \tag{5}$$

where E is the Young's modulus of the material and $I = \pi d^4/64$ is the section's moment of inertia.

Considering a distributed time-dependent external force $\boldsymbol{f}(x,t)$ that acts along the beam, its virtual work is

$$\delta W = \int_0^L \delta \boldsymbol{r}^T(x,t)\boldsymbol{f}(x,t)\mathrm{d}x \tag{6}$$

2.2 Spatial Discretization

Suppose that the beam is discretized into N elements with a set of arc-length coordinates of nodes $x_0, x_1, \ldots, x_{N-1}$. The length of the kth element is $\ell_k = x_k - x_{k-1}$. The position vector in the kth element can be interpolated by Hermite polynomials with the use of the position vector $\boldsymbol{r}$ and its slope vector $\boldsymbol{r}_x$ at discrete element nodes, and one has

$$\boldsymbol{r}(x,t) = s^\alpha(x)\boldsymbol{q}_{k_\alpha}(t), \quad \alpha = 1,2,3,4 \tag{7}$$

where the repeated indices must be interpreted as Einstein's implicit summation; and

$$\boldsymbol{q}_{k_1} = \boldsymbol{r}(x_{k-1},t), \quad \boldsymbol{q}_{k_2} = \boldsymbol{r}_x(x_{k-1},t), \quad \boldsymbol{q}_{k_3} = \boldsymbol{r}(x_k,t), \quad \boldsymbol{q}_{k_4} = \boldsymbol{r}_x(x_k,t) \tag{8}$$

are the kth element nodal coordinates; and s^α are the interpolation function that corresponds to each $\boldsymbol{q}_{k_\alpha}$, which are

$$s^1 = 1 - 3\xi^2 + 2\xi^3, \quad s^2 = \ell_k\left(\xi - 2\xi^2 + \xi^3\right), \quad s^3 = 3\xi^2 - 2\xi^3, \quad s^4 = \ell_k\left(\xi^3 - \xi^2\right) \tag{9}$$

where $\xi \in [0,1]$ is a non-dimensional coordinate defined within the element's length, such that $\xi = (x - x_{k-1})/\ell_k$. The differentiation of Eq. (7) with respect to time yields

$$\dot{\boldsymbol{r}}(x,t) = s^\alpha(x)\dot{\boldsymbol{q}}_{k_\alpha}(t) \tag{10}$$

Also, the first and second partial derivative of Eq. (7) with respect to x lead to

$$\boldsymbol{r}_x(x,t) = s_x^\alpha(x)\boldsymbol{q}_{k_\alpha}(t), \quad \boldsymbol{r}_{xx}(x,t) = s_{xx}^\alpha(x)\boldsymbol{q}_{k_\alpha}(t) \tag{11}$$

Therefore, using Eq. (10), the kinetic energy of the kth element of the beam can be expressed by

$$T = \frac{1}{2}\int_{x_k}^{x_{k+1}} \rho_A \dot{\boldsymbol{r}}^T \dot{\boldsymbol{r}} \mathrm{d}x = \frac{1}{2} m^{\alpha\beta} \dot{\boldsymbol{q}}_{k_\alpha}^T \dot{\boldsymbol{q}}_{k_\beta} \tag{12}$$

where $m^{\alpha\beta} = \int_{x_k}^{x_{k+1}} \rho_A s^\alpha s^\beta \mathrm{d}x$. When inextensibility is enforced, i.e., $\|\boldsymbol{r}_x\| \equiv 1$, the strain measure of Eq. (4) turns into $\kappa^2 = \|\boldsymbol{r}_{xx}\|^2$, which is in accordance with the commonly accepted approximation for the curvature of Euler-Bernoulli beams equal to the second-derivative of the transverse displacement (see for example Section 4.1 of [31]). The enforcement of inextensibility will be discussed in the Section 2.3. Therefore, it can be assumed that $\kappa^2 = \boldsymbol{r}_{xx} \cdot \boldsymbol{r}_{xx}$ in the discretization, substituting Eq. (11), one has

$$\kappa^2 = \chi^{\alpha\beta\mu\upsilon} Q_{\alpha\beta}(t) Q_{\mu\upsilon}(t) \tag{13}$$

where $Q_{\alpha\beta}(t) = \frac{1}{2}\boldsymbol{q}_{k_\alpha} \cdot \boldsymbol{q}_{k_\beta}$, and

$$\chi^{\alpha\beta\mu\upsilon} = 2\left(s_x^\alpha s_x^\beta s_{xx}^\mu s_{xx}^\upsilon + s_{xx}^\alpha s_{xx}^\beta s_x^\mu s_x^\upsilon\right) \tag{14}$$

Substituting Eq. (13) into Eq. (5), the elastic potential energy of the kth element of the beam is

$$U_k = \frac{1}{2} k^{\alpha\beta\mu\upsilon} Q_{\alpha\beta} Q_{\mu\upsilon} \tag{15}$$

where $k^{\alpha\beta\mu\upsilon} = \int_{x_k}^{x_{k+1}} EI\chi^{\alpha\beta\mu\upsilon}\mathrm{d}x$, which is the (constant) element of indices α, β, μ, and υ of the fourth-order stiffness tensor. The corresponding generalized elastic force is

$$\boldsymbol{Q}_e^\alpha = -\frac{\partial U_k}{\partial \boldsymbol{q}_{k_\alpha}} = -k^{\alpha\beta\mu\upsilon} Q_{\mu\upsilon} \boldsymbol{q}_{k_\beta} \tag{16}$$

The corresponding generalized external force is

$$\boldsymbol{Q}_f^\alpha = \frac{\partial \delta W_k}{\partial \delta \boldsymbol{q}_{k_\alpha}} = \int_{x_k}^{x_{k+1}} s^\alpha(x) \boldsymbol{f}(x,t) \mathrm{d}x \tag{17}$$

2.3 Constraint Equations

Since the centroid line of the beam is inextensible, the axial strain should be exactly zero. Without enforcing any constraint, this requirement cannot be satisfied at each discrete node and within elements due to the numerical drift of $\boldsymbol{r}_x$. Therefore, for the inextensible beam, the following nodal constraints are indispensable

$$\boldsymbol{C}_n: \quad \boldsymbol{r}_x(x_k,t)^T \boldsymbol{r}_x(x_k,t) - \mathring{\boldsymbol{r}}_x^T(x_k)\mathring{\boldsymbol{r}}_x(x_k) = 0, \quad k = 0,1,\dots,N \tag{18}$$

With the use of the nodal constraints, the axial deformation can be greatly restricted. However, the zero axial strain condition can still be violated within each beam element, causing moderate deformation drifting. Therefore, the integral of the axial strain along the centroid line at each time step must be satisfied. Suppose that the domain $[0, L]$ is divided into $\overline{n}$ subdomains, $[x_{k_0}, x_{k_1}]$, $[x_{k_1}, x_{k_2}]$, $\cdots$, $[x_{k_{\overline{n}-1}}, x_{k_{\overline{n}}}]$, where $x_{k_0} = x_0 = 0$ and $x_{k_{\overline{n}}} = x_{N-1} = L$. The constraint equations are

$$\boldsymbol{C}_i: \quad \int_{x_{k_j}}^{x_{k_{j+1}}} \left(\boldsymbol{r}_x(x,t)^T \boldsymbol{r}_x(x,t) - \mathring{\boldsymbol{r}}_x^T(x)\mathring{\boldsymbol{r}}_x(x)\right) \mathrm{d}x = 0, \quad j = 1,\dots,\overline{n} \tag{19}$$

where $j = 0,\dots,\overline{n}-1$. Note that the number of integration subdomains $\overline{n}$ is not necessarily the same as the number of beam elements, N. In cases where bending deformations are very small, a single constraint equation integrated along the whole beam is sufficiently accurate; when bending deformations are large, a constraint equation integrated over each element may be more favorable in terms of convergence.

Other kinematic constraints may connect bodies or enforce the movement; they are assumed to be holonomic and denoted by

$$\boldsymbol{C}_k: \boldsymbol{C}\big(\boldsymbol{q}, t\big) = \boldsymbol{0} \tag{20}$$

where $\boldsymbol{q}$ denotes the generalized coordinate vector that contains all the generalized nodal coordinates $\boldsymbol{q}_{k_\alpha}$.

Hence, the constraint equations of the system can be expressed by

$$\boldsymbol{c}(\boldsymbol{q}, t) = [\boldsymbol{C}_n; \boldsymbol{C}_i; \boldsymbol{C}_k] \tag{21}$$

The equations of motion can be written as Lagrange equations of the first kind as

$$\begin{gathered} \mathbf{M}\ddot{\boldsymbol{q}} + \boldsymbol{c}_{\boldsymbol{q}}^T \boldsymbol{\lambda} = \boldsymbol{F} \\ \mathbf{c}(\boldsymbol{q}, t) = \mathbf{0} \end{gathered} \tag{22}$$

where $\mathbf{M}$ represents the constant mass matrix that is composed of the elements' mass matrix coefficients $m^{\alpha\beta}$; $\boldsymbol{c}_{\boldsymbol{q}}$ is the derivative of $\boldsymbol{c}$ with respect to the generalized coordinates $\boldsymbol{q}$, i.e., the constraint Jacobian matrix; $\boldsymbol{\lambda}$ is the vector of the Lagrange multipliers; the load vector is $\boldsymbol{F} = \mathbf{Q}^e + \mathbf{Q}^f$, with $\mathbf{Q}^e$ and $\mathbf{Q}^f$ respectively originating from the combination of the generalized elastic force $\mathbf{Q}^e_\alpha$ resulting from the gradient of the potential energy and the generalized external force $\mathbf{Q}^f_\alpha$ acting on each element.

3 Explicit Integration Algorithm

In this section, a stabilization technique is adopted to transform the problem from the DAE form of Eqs. (22) into ODE form, such that it can be directly integrated using explicit schemes. The explicit Zhai method, proposed in [32], is briefly introduced and used throughout this work. The selection of the time step size, which greatly affects the efficiency of the integration, is discussed in detail.

3.1 Constraint Stabilization Procedure

To solve Eqs. (22) using explicit integration schemes, the problem must be transformed into ODE form by eliminating the Lagrange multipliers. Among the possible approaches, it is worth mentioning Baumgarte's stabilization technique [33], the so-called *Augmented Lagrangian* approach proposed by Bayo et al. [34], a self-stabilized algorithm proposed by Bauchau[35], or reduction to the minimal coordinate set using coordinate projection (see, for example, [36]).

In this work, the stabilization technique discussed in [6, 11] is used to transform a set of constraint equations into ODEs. A constraint equation,

$$f(t, \boldsymbol{x}) = 0 \tag{23}$$

can be converted into the ODE

$$\dot{f} + \zeta f = f_{\boldsymbol{x}}(t, \boldsymbol{x})\dot{\boldsymbol{x}} + f_t(t, \boldsymbol{x}) + \zeta f(t, \boldsymbol{x}) = 0 \tag{24}$$

where $\zeta > 0$ (dimensionally the inverse of a time) is a stabilization parameter. Its global asymptotically stable solution

$$f(t, \boldsymbol{x}) = f(t_0, \boldsymbol{x}) e^{-\zeta t} \tag{25}$$

approaches zero, $f = 0$, with exponential rate; ζ must be large enough to quickly pull back the drifting of the constraint onto the constraint manifold but not too large, to avoid the need for too short a time step for algorithmic stability when using explicit or conditionally stable integration methods.

By introducing an additional Lagrange multiplier $\boldsymbol{\mu}$, the index-3 DAEs of Eq. (22) can be transformed into index-2 ones with an affine invariant form [37] as

$$\mathbf{M}\dot{\boldsymbol{v}} + \boldsymbol{c}_{\boldsymbol{q}}^T \boldsymbol{\lambda} - \boldsymbol{F} = \mathbf{0} \tag{26a}$$

$$\mathbf{M}\dot{\boldsymbol{q}} + \boldsymbol{c}_{\boldsymbol{q}}^T \boldsymbol{\mu} - \mathbf{M}\boldsymbol{v} = \mathbf{0} \tag{26b}$$

$$\boldsymbol{c}_{\boldsymbol{q}}\boldsymbol{v} + \boldsymbol{c}_t = \mathbf{0} \tag{26c}$$

$$\boldsymbol{c}(\boldsymbol{q}, t) = \mathbf{0} \tag{26d}$$

where $\boldsymbol{\mu}$ can be interpreted as a projection term in the kinematic relationship between generalized coordinates and velocities; $\boldsymbol{v}$ denotes the generalized velocity.

Using the proposed stabilization technique, the third equation (26c) (i.e., the hidden velocity constraint equations) becomes

$$\mathbf{c}_{\boldsymbol{q}}\dot{\boldsymbol{v}} = \boldsymbol{\gamma} - \zeta\left(\mathbf{c}_{\boldsymbol{q}}\boldsymbol{v} + \mathbf{c}_t\right) \tag{27}$$

where

$$\boldsymbol{\gamma} = -\left(\mathbf{c}_{\boldsymbol{q}}\boldsymbol{v}\right)_{\boldsymbol{q}}\boldsymbol{v} - 2\mathbf{c}_{\boldsymbol{q}t}\boldsymbol{v} - \mathbf{c}_{tt}$$

and the fourth equation, Eq. (26d), i.e., the position constraint equation, becomes

$$\mathbf{c}_{\boldsymbol{q}}\dot{\boldsymbol{q}} = -\mathbf{c}_t - \zeta\mathbf{c} \tag{28}$$

Combining Eqs. (26a) (26b) with Eqs. (27) and (28), it yields the following form,

$$\begin{pmatrix} \mathbf{M}, & \mathbf{c}_{\boldsymbol{q}}^T \\ \mathbf{c}_{\boldsymbol{q}}, & \mathbf{0} \end{pmatrix}\begin{pmatrix} \dot{\boldsymbol{q}}, & \dot{\boldsymbol{v}} \\ \boldsymbol{\mu}, & \boldsymbol{\lambda} \end{pmatrix} = \begin{pmatrix} \mathbf{M}\boldsymbol{v}, & \boldsymbol{F} \\ -\mathbf{c}_t - \zeta\mathbf{c}, & \boldsymbol{\gamma} - \zeta\left(\mathbf{c}_{\boldsymbol{q}}\boldsymbol{v} + \mathbf{c}_t\right) \end{pmatrix} \tag{29}$$

which further yields

$$\begin{aligned} \dot{\boldsymbol{q}} &= \left(\mathbf{I} - \boldsymbol{\Gamma}\mathbf{c}_{\boldsymbol{q}}\right)\boldsymbol{v} - \boldsymbol{\Gamma}\left(\mathbf{c}_t + \zeta\mathbf{c}\right) \\ \dot{\boldsymbol{v}} &= \left(\mathbf{I} - \boldsymbol{\Gamma}\mathbf{c}_{\boldsymbol{q}}\right)\mathbf{M}^{-1}\boldsymbol{F} + \boldsymbol{\Gamma}\left(\boldsymbol{\gamma} - \zeta\left(\mathbf{c}_{\boldsymbol{q}}\boldsymbol{v} + \mathbf{c}_t\right)\right) \end{aligned} \tag{30}$$

where $\boldsymbol{\Gamma} = \mathbf{M}^{-1}\mathbf{c}_{\boldsymbol{q}}^T\boldsymbol{\Delta}^{-1}$ and $\boldsymbol{\Delta} = \mathbf{c}_{\boldsymbol{q}}\mathbf{M}^{-1}\mathbf{c}_{\boldsymbol{q}}^T$. Note that the mass matrix $\mathbf{M}$ in the present model is constant and its inverse can be calculated in advance.

Equations (30) constitute a set of first-order ODE equations for these states, which can be solved using the explicit Zhai method [32, 38, 39]. The right-hand sides of Eqs. (30) are evaluated from the generalized coordinates and velocities.

3.2 Explicit Zhai Method

The Zhai method [32] is briefly introduced. It is a predictor-corrector scheme combined with the Newmark method [40] to solve a set of second-order ODEs.

I. The generalized coordinates and velocities are predicted using the following equations:

$$\boldsymbol{q}_{p,n+1} = \boldsymbol{q}_n + \boldsymbol{v}_n + \left(\frac{1}{2} + \psi\right) \boldsymbol{a}_n \Delta t^2 - \psi \boldsymbol{a}_{n-1} \Delta t^2 \tag{31}$$

$$\boldsymbol{v}_{p,n+1} = \boldsymbol{v}_n + (1+\phi)\, \boldsymbol{a}_n \Delta t - \phi \boldsymbol{a}_{n-1} \Delta t \tag{32}$$

II. Accelerations are predicted by substituting the predicted generalized coordinates $\boldsymbol{q}_{p,n+1}$ and velocities $\boldsymbol{v}_{p,n+1}$ into the expression of the accelerations, namely the second of Eqs. (30).

III. The generalized coordinates and velocities are corrected using the Newmark method:

$$\boldsymbol{q}_{n+1} = \boldsymbol{q}_n + \boldsymbol{v}_n + \left(\frac{1}{2} - \beta\right) \boldsymbol{a}_n \Delta t^2 + \beta \boldsymbol{a}_{p,n+1} \Delta t^2 \tag{33}$$

$$\boldsymbol{v}_{n+1} = \boldsymbol{v}_n + (1-\gamma)\, \boldsymbol{a}_n \Delta t + \gamma \boldsymbol{a}_{p,n+1} \Delta t \tag{34}$$

where $\gamma \in (0,1)$ and $\beta = \frac{1}{4}\left(\frac{1}{2}+1\right)$.

IV. The acceleration $\boldsymbol{a}_{n+1}$ is evaluated from the second of Eqs. (30) with $\boldsymbol{q}_{n+1}$ and $\boldsymbol{v}_{n+1}$.

The correction of phase (III) can be omitted, yielding the simplest form of the explicit Zhai method. When $\psi = \phi = \frac{1}{2}$, no algorithmic dissipation is introduced [32].

3.3 Step Size Selection Strategy

For the extensible beam, the axial vibration frequencies are usually much higher than those associated with bending, which limits the step size that can be used with the explicit integration scheme to meet the algorithmic stability requirements. In the proposed inextensible beam model, the bending vibration frequency of an element is of the order of

$$\omega \sim \frac{1}{l_e^2}\sqrt{\frac{EI}{\rho A}} \tag{35}$$

where l_e is the length of the element. The time step size needs to meet the requirement

$$h\omega \le C \tag{36}$$

where C is a constant parameter that is less than 1. Substituting Eq. (35) in Eq. (36) leads to

$$h \le \frac{C}{\omega} = l_e^2 \frac{C}{\alpha^2}\sqrt{\frac{EI}{\rho A}} = h_{\max} \tag{37}$$

where α is a constant parameter ($\alpha \approx 3\pi/2$ for an isolated element, under free-free boundary conditions). Equation (37) represents the maximum step size $h_{\max}$ that can be used in the simulation. It also shows that the maximum time step size is proportional to the square of the length of the element, $h \sim l_e^2$.

The stabilization algorithm introduces another limitation on the time step size, $h_{\max} \sim 1/\zeta$. The inextensibility kinematic constraint eliminates the bound on the time step imposed by the physical high-frequency axial dynamics. However, to enable the use of explicit algorithms, the problem must be transformed into an ODE system using a stabilization algorithm, which also imposes a limitation on the time-step size. A trade-off must be found by choosing a value of ζ less restrictive than the original axial dynamics, while effectively keeping the constraint drift bounded.

4 Numerical Examples

In this section, to validate the capabilities of the proposed ANCF model and the efficiency of explicit integration for inextensible beams, four benchmark examples are analyzed. They are:

4.1 The forced vibrations of a ring, a problem used to validate the accuracy of the proposed approach and verify the effectiveness of the step size selection strategy.

4.2 A 2D flexible pendulum, where the performances of both the conventional and present ANCF are compared, illustrating accessible large step sizes in the current approach.

4.3 A 3D flexible pendulum, used to validate the capability of the present formulation in spatial problems.

4.4 An engineering problem, i.e., a power transmission line, is used to validate the effectiveness of the proposed method in more complex scenarios.

4.1 Vibrating Ring

The vibrations of a flexible ring under harmonic external forces, originally proposed in [27], are investigated. As shown in Fig. 1, the ring's initial position is described by

$$\boldsymbol{z}_0(\theta) = R\,(\cos\theta, \sin\theta)\,, \tag{38}$$

where $\theta \in [0, 2\pi]$ and $R = 0.5$ m. A pair of harmonic forces with equal magnitude and opposite directions

$$F = F_0 \sin(\omega t) \tag{39}$$

act at points N_1 and N_2, respectively, where $F_0 = 10$ N and $\omega = 10\pi$ radian/s. The cross-section of the ring is circular with radius 5×10^{-3} m, density $\rho = 2700$ kg/m^3, and Young's modulus $E =$ 7.0 GPa.

The problem is integrated with the explicit Zhai method using the modified ANCF model with 20 elements. According to Eq. (37), the time step size is $h = 2.4842 \times 10^{-4}$ s, where the constant parameter $C = 0.9$ and $\alpha = \frac{3}{2}\pi$. In addition, the stabilization parameter ζ is set to 100 s^{-1}. The simulation results of the radial displacement at point N_1 are compared to the corresponding ones obtained using MBDyn[1], a free, general-purpose multibody solver [41]. In the latter case, the ring is discretized using 40 three-node beam elements and integrated using a two-step linear implicit multistep scheme with tunable algorithmic dissipation (LMS2 [42, 43], with asymptotic spectral radius $\rho_\infty = 0.6$) also using a step size $h = 2.4842 \times 10^{-4}$ s.

[1] `https://mbdyn.org/`, last accessed March 2025.

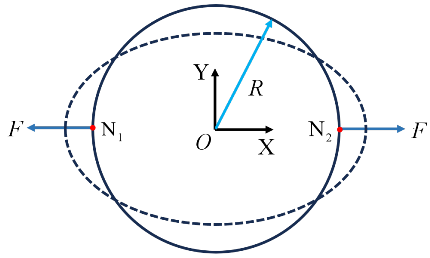

Figure 1: Vibrating ring: problem description.

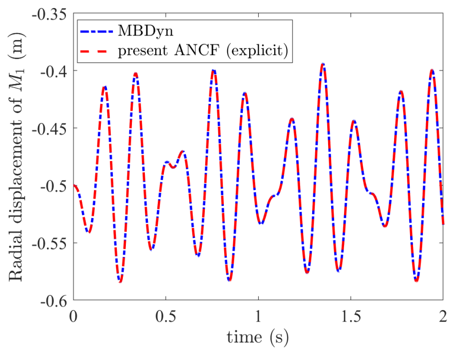

Figure 2: Vibrating ring: radial displacement at point N_1

As depicted in Fig. 2, the results of the proposed method are in good agreement with those obtained using MBDyn, verifying the capabilities of the proposed approach.

Figure 3 shows snapshots of the evolution at different times (from left to right and top to bottom), where the ring oscillates periodically with symmetric displacement in the north-south direction and alternating directions in the east-west direction.

4.2 Planar Flexible Pendulum

To illustrate the efficient explicit simulation featured by the current approach, a flexible pendulum that can be assumed to be an inextensible beam is considered here. The numerical results are compared with the corresponding ones from an explicit simulation based on the conventional ANCF formulation.

Consider a single pendulum with $L = 1.8$ m, with a uniform gravity field $g = 9.81$ m/s^2 along the negative z axis. The density is $\rho = 2766.76$ kg/m^3 and the radius is $R = 2 \times 10^{-3}$ m. The elastic modulus is $E = 6.895$ GPa. The pendulum is connected to the ground by a revolute joint at the origin. The initial position of the pendulum's endpoint is $\boldsymbol{r} = [L, 0, 0]$, with initial velocity $\dot{\boldsymbol{r}} = [0, 0, 0]$ m/s and initial angular velocity $\boldsymbol{\omega}_0 = [0, 0, 0]$ rad/s. The pendulum rotates about axis y in the plane x–z, as sketched in Fig. 4.

Table 1: Planar flexible pendulum: computational time

Formulations	Conventional ANCF element		Proposed ANCF element
Integrators	implicit	explicit	explicit
Time (s)	1.649	120.9	0.680

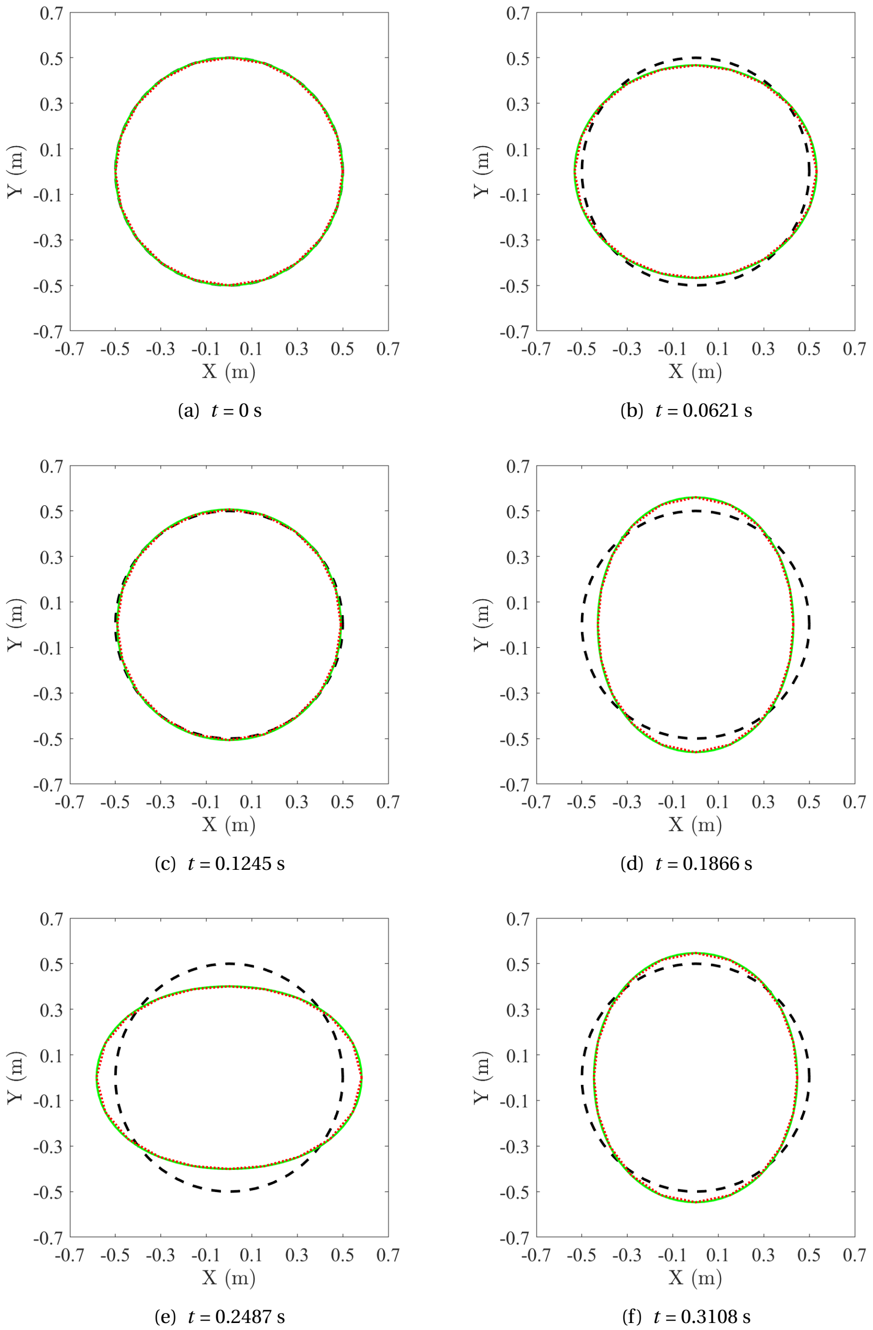

Figure 3: Vibrating ring: evolution of the solution at different times between current approach (red dot line) and MBDyn (green line), with the undeformed ring configuration (black dash line).

The problem is solved by applying the explicit Zhai integration scheme to the present and conventional ANCF formulations. The results are compared to the corresponding ones obtained using the generalized-α integrator applied to the conventional ANCF formulation. In the present ANCF

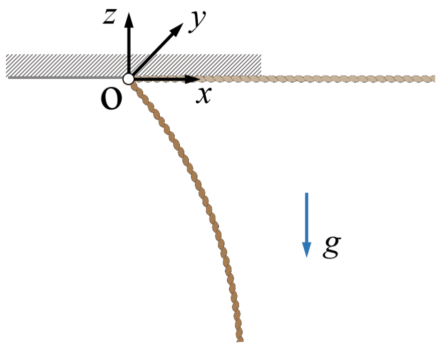

Figure 4: Planar flexible pendulum: problem description.

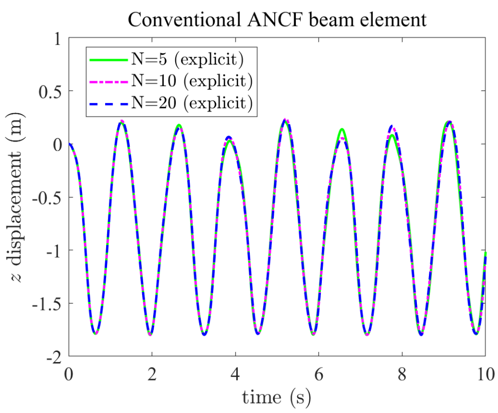

Figure 5: Planar flexible pendulum: discretization convergence of the explicit solution based on the conventional ANCF formulation.

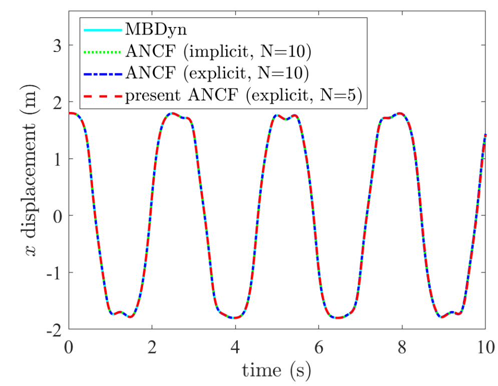

(a) x displacement

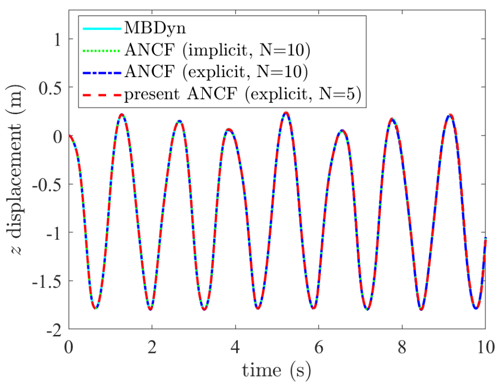

(b) z displacement

Figure 6: Planar flexible pendulum: endpoint coordinates, comparison of different solution approaches.

formulation, 5 elements are used. In the explicit Zhai method, the time step size is $h = 2.6 \times 10^{-3}$ s, which is obtained using Eq. (37) with the constant parameter $C = 0.7$, and the number of integration subdomains is $\overline{n} = 5$. In the conventional ANCF formulation, as shown in Fig. 5 where simulation results are compared with different numbers of elements, at least 10 elements are required to obtain the convergent simulation result. In the explicit Zhai method, the maximum time step size is $h = 2 \times 10^{-5}$ s. In both cases, a stabilization parameter $\zeta = 100\ \mathrm{s}^{-1}$ is used. To compare with implicit integration schemes, the problem is also solved using the generalized-α integrator with a constant step size $h = 5 \times 10^{-3}$ s and 10 conventional ANCF elements. The results are compared with the corresponding ones from MBDyn, where a model with 10 three-node beam elements is integrated with a time step size $h = 10^{-3}$ s. The resulting endpoint displacement components are depicted in Fig. 6, which shows good agreement between the output of the different solvers.

Due to the merits of the current ANCF model for inextensible beams, smaller numbers of elements can be used, and the stiffness of dynamic equations is reduced, allowing larger time step sizes in the explicit simulation. Both the smaller number of ANCF elements and larger step sizes contribute to the efficiency. As in Table 1, the explicit simulation of the present ANCF model is much more efficient than that of the conventional one, and is also faster than the simulation by the implicit generalized-α method, validating the present ANCF formulation.

4.3 Spatial Flexible Pendulum

To further verify the current formulation when applied to spatial problems, a three-dimensional flexible pendulum with the same parameters presented in Section 4.2 is analyzed. The pendulum is now connected to the ground by a spherical hinge, and has an initial velocity that grows linearly along the y-axis from zero at the attachment point to $\boldsymbol{v}_0 = 3.0$ m/s at the free end.

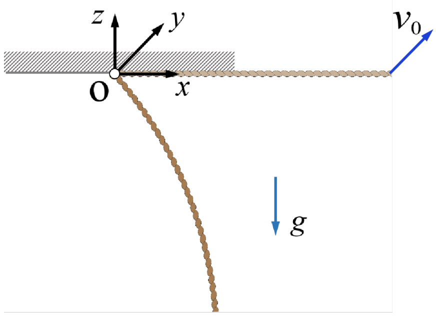

Figure 7: Spatial flexible pendulum: problem description.

The dynamics are modeled using the proposed ANCF formulation with 5 elements and integrated with the previously mentioned explicit integration scheme. The number of integration subdomains is $\overline{n} = 5$, the time step size is $h = 10^{-3}$ s, and the stabilization parameter is $\zeta = 1000\ \mathrm{s}^{-1}$. The endpoint trajectory closely matches the corresponding one calculated by MBDyn, as shown in Fig. 8, which uses a model with 10 three-node beam elements integrated with a time step size of $h = 10^{-3}$ s. To compare the proposed ANCF beam formulation with the conventional one, a discretization convergence analysis of the conventional ANCF beam model is performed. The y component of the pendulum's endpoint position is computed using the explicit integrator with a varying number of element, a time step of $h = 2 \times 10^{-5}$ s, and a stabilization parameter of $\zeta = 1000\ \mathrm{s}^{-1}$. The simulation results, shown in Fig. 9, indicate that approximately 10 conventional ANCF beam elements are required for convergence.

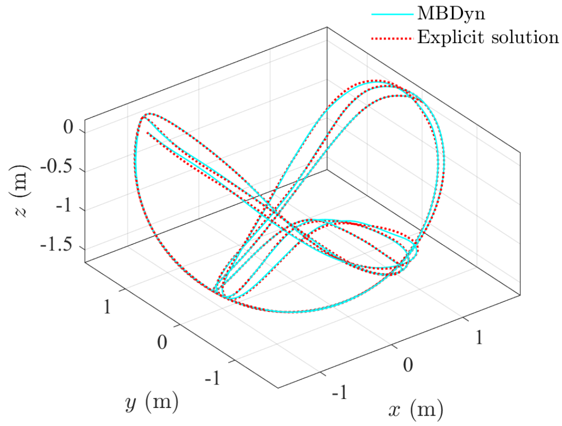

Figure 8: Spatial pendulum: discretization convergence of the explicit solution based on the conventional ANCF formulation

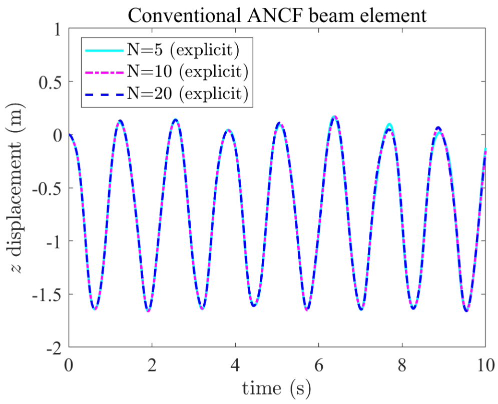

Figure 9: Spatial pendulum: discretization convergence of the explicit solution based on the conventional ANCF formulation

To further compare efficiency, the dynamics modeled with 10 conventional ANCF beam elements are also computed using the implicit generalized-α integrator ($h = 2 \times 10^{-3}$ s). The endpoint displacements obtained from the different approaches are shown in Fig. 10, demonstrating good agreement with MBDyn. Additionally, Fig. 10 highlights the superiority of the proposed ANCF beam model for inextensible beams over the conventional one, as it requires fewer elements to achieve the same computational accuracy. Furthermore, compared to the conventional ANCF model, the proposed formulation allows for larger time step sizes when using the explicit Zhai integrator.

Table 2 provides the computational time of different approaches, showing that the explicit simulation of the present ANCF model is much more efficient than that of the conventional one, and is also faster than the simulation by the implicit generalized-α method, validating the present ANCF formulation.

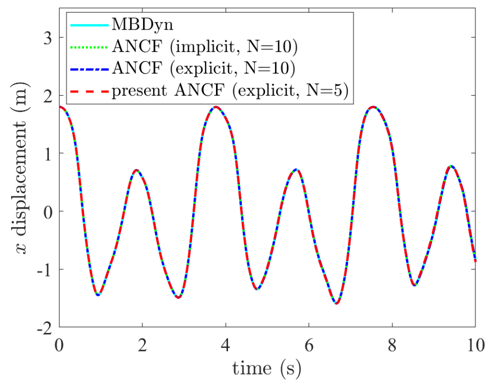

(a) x displacement

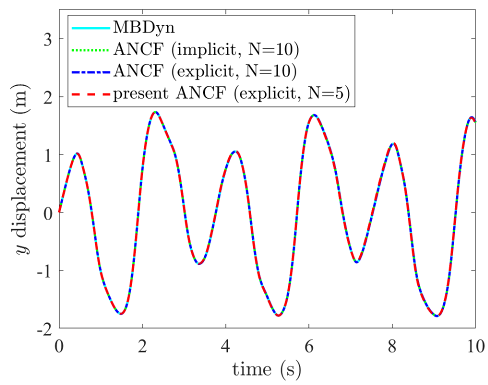

(b) y displacement

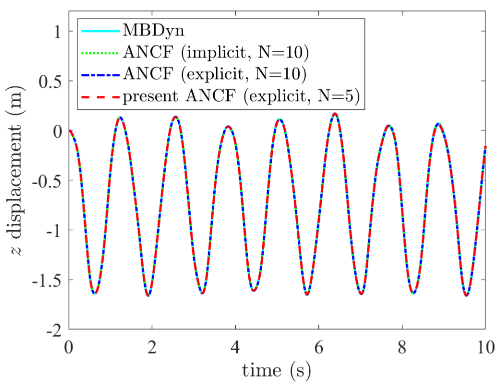

(c) z displacement

Figure 10: Spatial flexible pendulum: endpoint position components

Table 2: Spatial flexible pendulum: computational time

Formulations	Conventional ANCF element		Proposed ANCF element
Integrators	implicit	explicit	explicit
Time (s)	3.6090	301.71	1.8502

4.4 Power Transmission Line

Ice can form on power transmission lines [44]; their dynamic response when ice sheds can be used as a benchmark to validate the proposed method. The two-span transmission line in Fig. 11 is studied. The power transmission line is assumed to be made of a stainless steel strand with a circular cross-section of about 2 mm radius.

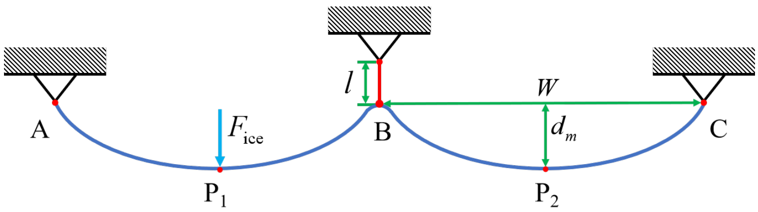

Figure 11: Power transmission line: problem description.

The displacements at the endpoints A and C of the line are fixed. In the reference configuration, the three points A, B, and C are at the same height; point B is at mid span between points A and C. The width between points B and C is $W = 3.322$ m. The total length of the power transmission line is $L = 6.7036$ m. The line is hung at point B by a freely swinging rigid insulator of length $l = 0.1$ m. When ice is not present, the power transmission line sags under gravity and reaches an equilibrium position, forming spans 1 and 2. The lowest points of spans 1 and 2 are P_1 and P_2, respectively. Suppose a block of ice forms at point P_1, approximated by a lumped mass whose weight $F_{ice} = 1.162$ N acts on that point of the line. The linear spanwise density is $\rho_A = 9.26 \times 10^{-2}$ kg/m and the bending stiffness is $EI = 2.1113$ N·m^2. A gravitational acceleration $g = 9.81$ m/s^2 is considered.

When there is no ice and the power line is only subject to its weight, the configuration of each span can be initially approximately by a parabola, such that the maximum sag d_m at points P_1 and P_2 can be expressed by

$$d_m = \sqrt{\frac{3(L-2W)W}{16}} \tag{40}$$

Using the parabolic configuration of Eq. (40) as initial undeformed configuration, the equilibrium configuration under the action of gravity can be obtained by solving the static equation using Newton's iteration. This solution is the blue solid line shown in Fig. 12. Similarly, starting from the configuration deformed under gravity, the equilibrium configuration under the action of the concentrated ice force can be calculated. This solution is the dashed red line in Fig. 12.

A sudden shedding of the ice while at equilibrium would cause an unbalance, resulting in a dynamic response of the power transmission line. The large deformations and displacements of the wire are formulated using the current ANCF beam model integrated with the explicit Zhai method and compared to the conventional ANCF model (with axial stiffness $EA = 1490955$ N) integrated using the same explicit method.

In the modified formulation, 20 elements are used, with a time step $h = 9.35 \times 10^{-4}$ s, deter-

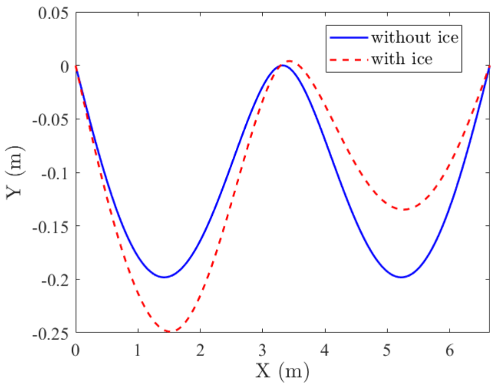

Figure 12: Power transmission line: equilibrium configurations with and without ice.

mined from Eq. (37) with $C = 0.85$. The number of integration subdomains is $\overline{n} = 20$. In contrast, the conventional formulation requires at least 40 elements to achieve comparable accuracy, with a maximum time step $h = 10^{-5}$ s. In both cases, the stabilization parameter is $\zeta = 1000\ \mathrm{s}^{-1}$. The simulation results, shown in Fig. 13, are compared with those obtained using ABAQUS. In ABAQUS, 1004 quadratic beam elements of type B22 are used to achieve convergence. A static analysis is first conducted to determine the initial equilibrium configuration, followed by an implicit dynamic analysis to compute the response after ice shedding. The latter employs an adaptive variable-step integration scheme with a maximum time step $h = 10^{-3}$ s. The results show strong agreement, validating the effectiveness of the proposed approach.

The computational times of the conventional and proposed ANCF beam elements are compared in Table 3. The results show that the proposed ANCF with explicit integration is approximately 200 times faster than the conventional one, demonstrating the significant efficiency of the explicit simulation for inextensible beams in analyzing the dynamics of complex mechanical systems.

Table 3: Power transmission line: computational time.

Formulations	conventional ANCF element	present ANCF element
Integrators	explicit	explicit
Time (s)	3593.8	17.28

5 Conclusions

In this work, an efficient explicit integration method for inextensible flexible beams is developed using a new ANCF beam model. The study demonstrates that the proposed model enables significantly larger time steps in explicit schemes compared to conventional ANCF formulations. Numerical examples validate its effectiveness, showing that, with an appropriate step-size selection strategy, the permissible step size can be nearly 100 times larger than that of the conventional ANCF model. As a result, the proposed approach enhances computational efficiency by approximately two orders of magnitude in explicit simulations.

The derivation of the proposed formulation shares similarities with the conventional gradient-deficient ANCF, as both rely on nodal position coordinates and their slope vectors. In this sense, the

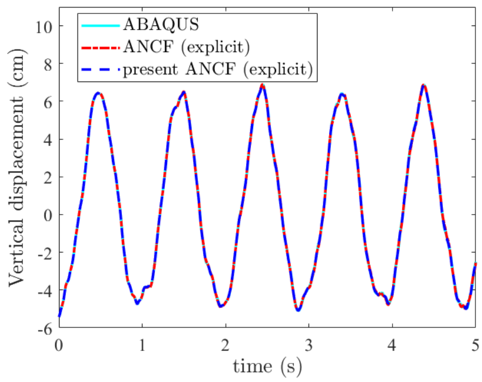

(a) Vertical displacement of point P_1

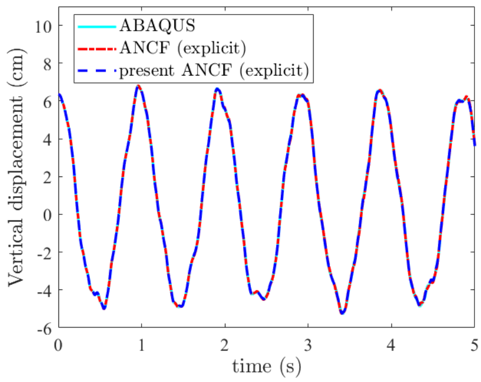

(b) Vertical displacement of point P_2

Figure 13: Power transmission line: vertical component of the position of the two spans' lowest points, P_1 and P_2.

proposed model can be regarded as an advanced gradient-deficient ANCF formulation. However, it introduces two key improvements: 1) the elastic potential energy is directly derived from the squares of the first and second derivatives of the position vector with respect to the arc-length coordinate, leading to equations of motion with moderate stiffness. 2) the inextensibility condition is rigorously enforced through algebraic constraints on the slope vectors at discrete element nodes, along with fixed-length constraints. These enhancements make the proposed model particularly well-suited for explicit integration schemes.

The advantages of this work are:

- The proposed ANCF model provides an effective dynamic representation of inextensible beams.
- Larger step sizes can be used in explicit schemes compared to existing ANCF formulations.
- An appropriate time step can be determined using the proposed step size selection strategy.
- Computational efficiency is significantly improved, making real-time simulations more feasible.

The main drawback of the proposed approach is the need to enforce algebraic constraints at each node, increasing the number of equations to be solved. However, because of its ability to

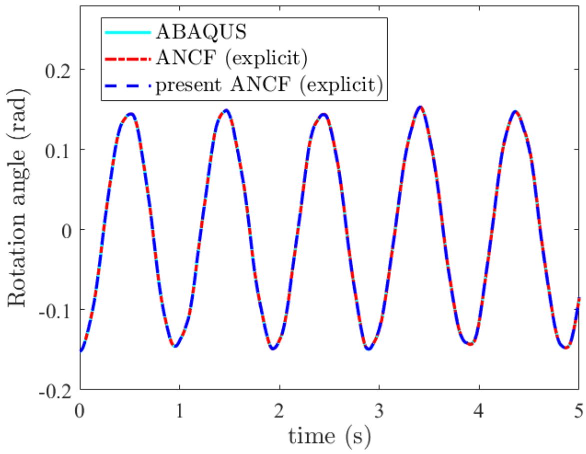

Figure 14: Power transmission line: rotation of the line at point C.

use large step sizes, high explicit efficiency can be achieved. Combined with its potential for high parallel computation, overall computational efficiency can be further enhanced.

The proposed method is particularly suited for explicit simulations of inextensible beam or cable systems subject to holonomic constraints, such as wire-rope systems. With parallel computing, real-time simulation becomes achievable. Although this work focuses on the explicit Zhai method, the proposed framework is compatible with other explicit schemes as well.

Data availability

All data generated or analyzed during this study are included in this article.

Declarations

Conflict of interest The authors declare that they have no conflict of interest.

Acknowledgments

Supported by the National Natural Science Foundation of China (Grant No.12402045), China Postdoctoral Science Foundation (Grant No.2024M754168), and Heilongjiang Postdoctoral Fund (LBH-Z24186).

References

[1] Narges Mohammadi, Asko Rouvinen, Pasi Korkealaakso, and José L. Escalona. Real-time explicit co-simulation of wire-rope systems for industrial mobile harbor cranes. *Nonlinear Dynamics*, 112(15):13095–13114, August 2024. https://doi.org/10.1007/s11071-024-09752-z.

[2] Ivan Maurović, Mato Baotić, and Ivan Petrović. Explicit model predictive control for trajectory tracking with mobile robots. In *2011 IEEE/ASME International Conference on Advanced Intelligent Mechatronics (AIM)*, pages 712–717, Budapest, Hungary, 2011. https://doi.org/10.1109/AIM.2011.6027140.

[3] Cheng Chen, James M. Ricles, Thomas M. Marullo, and Oya Mercan. Real-time hybrid testing using the unconditionally stable explicit CR integration algorithm. *Earthquake Engineering & Structural Dynamics*, 38(1):23–44, 2009. https://doi.org/10.1002/eqe.838.

[4] DS Bae, JK Lee, HJ Cho, and H Yae. An explicit integration method for realtime simulation of multibody vehicle models. *Computer Methods in Applied Mechanics and Engineering*, 187(1–2):337–350, 2000. https://doi.org/10.1016/S0045-7825(99)00138-3.

[5] Yongjun Pan, Saidi Xiang, Yansong He, Jian Zhao, and Aki Mikkola. The validation of a semi-recursive vehicle dynamics model for a real-time simulation. *Mechanism and Machine Theory*, 151:103907, 2020. https://doi.org/10.1016/j.mechmachtheory.2020.103907.

[6] Ping Zhou and Hui Ren. Stabilized explicit integrators for local parametrization in multi-rigid-body system dynamics. *Journal of Computational and Nonlinear Dynamics*, 17(10):101005, 2022. https://doi.org/10.1115/1.4054801.

[7] Ahmed A. Shabana, Dayu Zhang, and Gengxiang Wang. TLISMNI/Adams algorithm for the solution of the differential/algebraic equations of constrained dynamical systems. *Proceedings of the Institution of Mechanical Engineers Part K-Journal of Multi-Body Dynamics*, 232(1):129–149, 2018. https://doi.org/10.1016/j.jsv.2015.05.008.

[8] Q. X. Liu, J. K. Liu, and Y. M. Chen. An explicit hybrid method for multi-term fractional differential equations based on Adams and Runge-Kutta schemes. *Nonlinear Dynamics*, 84(4):2195–2203, June 2016. https://doi.org/10.1007/s11071-016-2638-z.

[9] V. Brasey and E. Hairer. Symmetrized half-explicit methods for constrained mechanical systems. *Applied Numerical Mathematics*, 13(1–3):23–31, 1993. https://doi.org/10.1016/0168-9274(93)90128-E.

[10] Bassam Hussein, Dan Negrut, and Ahmed A. Shabana. Implicit and explicit integration in the solution of the absolute nodal coordinate differential/algebraic equations. *Nonlinear Dynamics*, 54(4):283–296, 2008. https://doi.org/10.1007/s11071-007-9328-9.

[11] Hui Ren and Ping Zhou. A fast explicit integrator for numerical simulation of multibody system dynamics. In Andrés Kecskeméthy and Francisco Geu Flores, editors, *Multibody Dynamics 2019*, pages 348–355, Cham, 2020. Springer International Publishing. https://doi.org/10.1007/978-3-030-23132-3_42.

[12] G. M. Hulbert and J.T. Chung. Explicit time integration algorithms for structural dynamics with optimal numerical dissipation. *Computer Methods in Applied Mechanics and Engineering*, 137(2):175–188, 1996. https://doi.org/10.1016/S0045-7825(96)01036-5.

[13] WJT Daniel. Explicit/implicit partitioning and a new explicit form of the generalized alpha method. *Communications in Numerical Methods in Engineering*, 19(11):909–920, 2003. https://doi.org/10.1016/B978-0-08-043981-5.50010-9.

[14] Holger Lang, Joachim Linn, and Martin Arnold. Multi-body dynamics simulation of geometrically exact Cosserat rods. *Multibody System Dynamics*, 25(3):285–312, 2011. https://doi.org/10.1007/s11044-010-9223-x.

[15] Zheng Chen, Hui Ren, Wei Fan, and Ping Zhou. A new recursive geometrically exact formulation for three-dimensional Euler-Bernoulli beams with large deformations. *Nonlinear Dynamics*, 113:4671–4701, 2025. https://doi.org/10.1007/s11071-024-10409-0.

[16] Jian Qi Zou, Jing Jun Zhang, You Fang Lu, and Bin Wang. An explicit recursive formulation and parallel computation for inverse dynamics of planar flexible manipulators. In *ISIE '97 Proceeding of the IEEE International Symposium on Industrial Electronics*, pages 906–909, Guimaraes, Portugal, 1997. https://doi.org/10.1109/ISIE.1997.648843.

[17] Frank Naets, Tommaso Tamarozzi, Gert H. K. Heirman, and Wim Desmet. Real-time flexible multibody simulation with global modal parameterization. *Multibody System Dynamics*, 27(3):267–284, 2012. https://doi.org/10.1007/s11044-011-9298-z.

[18] Yancong Wang, Yifan Qin, Kai Luo, Qiang Tian, and Haiyan Hu. Dynamic modeling and simulation of hard-magnetic soft beams interacting with environment via high-order finite elements of ANCF. *International Journal of Engineering Science*, 202:104102, 2024. https://doi.org/10.1016/j.ijengsci.2024.104102.

[19] Qinglong Tian, Hongyu Sun, and Zuqing Yu. Model order reduction of thermal-dynamic coupled flexible multibody system with multiple varying parameters. *Applied Mathematical Modelling*, 136:115634, 2024. https://doi.org/10.1016/j.apm.2024.08.006.

[20] Peng Lan, Qinglong Tian, and Zuqing Yu. A new absolute nodal coordinate formulation beam element with multilayer circular cross section. *Acta Mechanica Sinica*, 36(1):82–96, February 2020. https://doi.org/10.1007/s10409-019-00897-4.

[21] Yimin Tang, Jianqiao Guo, Qiang Tian, and Haiyan Hu. Dynamic modeling of three-dimensional muscle wrapping based on absolute nodal coordinate formulation. *Nonlinear Dynamics*, 112(15):13073–13093, 2024. https://doi.org/10.1007/s11071-024-09754-x.

[22] Mohil Patel and Ahmed A. Shabana. Locking alleviation in the large displacement analysis of beam elements: the strain split method. *Acta Mechanica*, 229(7):2923–2946, 2018. https://doi.org/10.1007/s00707-018-2131-5.

[23] Johannes Gerstmayr and Ahmed A. Shabana. Analysis of thin beams and cables using the absolute nodal coordinate formulation. *Nonlinear Dynamics*, 45(1–2):109–130, 2006. https://doi.org/10.1007/s11071-006-1856-1.

[24] Wei Fan, Songhan Zhang, Weidong Zhu, and Hao Zhu. An efficient dynamic formulation for the vibration analysis of a multi-span power transmission line excited by a moving deicing robot. *Applied Mathematical Modelling*, 103:619–635, March 2022. https://doi.org/10.1016/j.apm.2021.10.040.

[25] Ping Zhou, Hui Ren, Wei Fan, and Zexu Zhang. A spacetime variational integration approach to the full discretization of flexible beams based on absolute nodal coordinate formulation. *Nonlinear Dynamics*, 113:1175–1190, 2025. https://doi.org/10.1007/s11071-024-10305-7.

[26] Ping Zhou, Hui Ren, Wei Fan, and Zexu Zhang. Variational integration approach for arbitrary Lagrangian-Eulerian formulation of flexible cables. *Applied Mathematical Modelling*, 138:115820, 2025. https://doi.org/10.1016/j.apm.2024.115820.

[27] Sören Bartels. A simple scheme for the approximation of elastic vibrations of inextensible curves. *IMA Journal of Numerical Analysis*, 36(3):1051–1071, 2016. https://doi.org/10.1093/imanum/drv054.

[28] Wei Fan and Weidong Zhu. An accurate singularity-free formulation of a three-dimensional curved Euler-Bernoulli beam for flexible multibody dynamic analysis. *Journal of Vibration and Acoustics*, 138(5):051001, 2016. https://doi.org/10.1115/1.4033269.

[29] Wei Fan, Hui Ren, Weidong Zhu, and Hao Zhu. Dynamic analysis of power transmission lines with ice-shedding using an efficient absolute nodal coordinate beam formulation. *Journal of Computational and Nonliear Dynamics*, 16(1):011005, 2021. https://doi.org/10.1115/1.4048361.

[30] Johannes Gerstmayr and Hans Irschik. On the correct representation of bending and axial deformation in the absolute nodal coordinate formulation with an elastic line approach. *Journal of Sound and Vibration*, 318(3):461–487, 2008. https://doi.org/10.1016/j.jsv.2008.04.019.

[31] Jacques Heyman. *Structural Analysis — A Historical Approach*. Cambridge University Press, Cambridge, 1998. https://doi.org/10.1017/CBO9780511529580.

[32] Wanming Zhai. Two simple fast integration methods for large-scale dynamic problems in engineering. *International Journal for Numerical Methods in Engineering*, 39(24):4199–4214, 1996. https://doi.org/10.1002/(SICI)1097-0207(19961230)39:24<4199::AID-NME39>3.0.CO;2-Y.

[33] J. Baumgarte. Stabilization of constraints and integrals of motion in dynamical systems. *Computer Methods in Applied Mechanics and Engineering*, 1(1):1–16, 1972. https://doi.org/10.1016/0045-7825(72)90018-7.

[34] E. Bayo, J. García de Jalón, and M. A. Serna. A modified Lagrangian formulation for the dynamic analysis of constrained mechanical systems. *Comput. Meth. Appl. Mech. Engng.*, 71(2):183–195, 1988. https://doi.org/10.1016/0045-7825(88)90085-0.

[35] Olivier A. Bauchau. A self-stabilized algorithm for enforcing constraints in multibody systems. *International Journal of Solids and Structures*, 40(13):3253–3271, 2003. https://doi.org/10.1016/S0020-7683(03)00159-8.

[36] Ping Zhou, Andrea Zanoni, and Pierangelo Masarati. A projection continuation approach for minimal coordinate set constrained dynamics. *Multibody System Dynamics*, 57(3–4):237–257, 2023. https://doi.org/10.1007/s11044-023-09882-z.

[37] C. W. Gear, B. Leimkuhler, and G. K. Gupta. Automatic Integration of Euler-Lagrange Equations with Constraints. *J. Comput. Appl. Math.*, 12–13:77–90, 1985. https://doi.org/10.1016/0377-0427(85)90008-1.

[38] Wanming Zhai. *Numerical Method and Computer Simulation for Analysis of Vehicle–Track Coupled Dynamics*, pages 203–229. Springer Singapore, Singapore, 2020. https://doi.org/10.1007/978-981-32-9283-3_4.

[39] Wanming Zhai, He Xia, Chengbiao Cai, Mangmang Gao, Xiaozhen Li, Xiangrong Guo, Nan Zhang, and Kaiyun Wang. High-speed train-track-bridge dynamic interactions-Part I: theoretical model and numerical simulation. *International Journal of Rail Transportation*, 1(1–2):3–24, 2013. https://doi.org/10.1080/23248378.2013.791498.

[40] Nathan M. Newmark. A method of computation for structural dynamics. *Journal of the Engineering Mechanics Division*, 85(3):67–94, 1959. 10.1061/JMCEA3.0000098.

[41] Pierangelo Masarati, Marco Morandini, and Paolo Mantegazza. An efficient formulation for general-purpose multibody/multiphysics analysis. *J. Comput. Nonlin. Dyn.*, 9(4):041001, 2014. https://doi.org/10.1115/1.4025628.

[42] Huimin Zhang, Runsen Zhang, and Pierangelo Masarati. Improved second-order unconditionally stable schemes of linear multi-step and equivalent single-step integration methods. *Computational Mechanics*, 67(1):289–313, 2021. https://doi.org/10.1007/s00466-020-01933-y.

[43] Huimin Zhang, Runsen Zhang, Andrea Zanoni, and Pierangelo Masarati. Performance of implicit A-stable time integration methods for multibody system dynamics. *Multibody System Dynamics*, 54(3):263–301, 2022. https://doi.org/10.1007/s11044-021-09806-9.

[44] A. Jamaleddine, G. McClure, J. Rousselet, and R. Beauchemin. Simulation of ice-shedding on electrical transmission lines using adina. *Computers & Structures*, 47(4–5):523–536, 1993. https://doi.org/10.1016/0045-7949(93)90339.